Stretching and Bending Moduli of Bilayer Films Inferred from Wrinkle Patterns

Jooyoung Chang[1], Narayanan Menon[2], and Thomas P. Russell[1,*]

[1]Department of Polymer Science and Engineering,

[2]Department of Physics,

University of Massachusetts Amherst, MA 01003

*Corresponding Author: russell@mail.pse.umass.edu

For Table of Contents use only

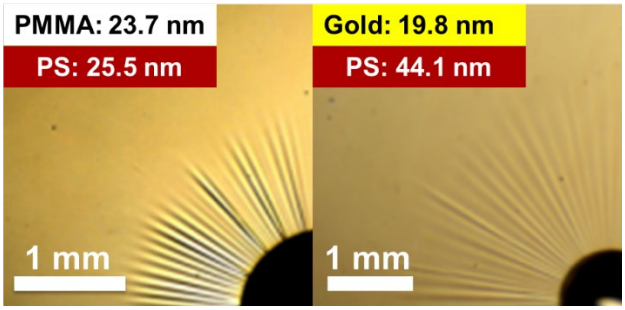

Abstract

Wrinkling patterns were used to investigate the mechanical properties of thin poly(styrene) (PS)/poly(methylmethacrylate) (PMMA) and PS/gold (Au) bilayer films. Films were floated on water with a water drop on the surface to induce wrinkling. The thicknesses and thickness ratios of the films were varied over a broad range. The PS/PMMA bilayer was chosen to provide a contrast in wetting properties, with equilibrium contact angles of θ_{PMMA} = 68º and θ_{PS} = 88º with water. The PS/Au bilayer was chosen to provide a large contrast in Young's moduli, E_{Au}= 72 GPa and E_{PS}= 3.4 GPa. The stretching (Y) and bending (B) moduli of the bilayer films were obtained from measurements of the length and the number of wrinkles in the wrinkle patterns. The experimentally derived values of Y and B were in reasonable agreement with the values computed

from the bulk Young's moduli and the thicknesses of the two components in the bilayer. The values of Y and B did not depend on which face of the film was exposed to the water droplet or bath when the capillary stresses were considered. Thus, finite size effects from the film thicknesses were unimportant over the range of thicknesses studied, and no relative displacement of the films was found, with the films remaining well-bonded even with the deformation associated with wrinkling.

Introduction

Due to the rapid growth in demand for small-scale devices, multilayer nanoscale structures have been used extensively as a key element in the design and performance of devices. Therefore, accurate determination of mechanical properties of the multi-layer films is necessary. Elucidation of the strength and the reliability of these devices with current nanotechnologies has been extremely challenging. This is of importance for the design, processing, testing, and packaging of flexible electronic devices, semi-conductors, photoresists, solar cells, and coatings. Different organic, polymeric, polymer-metal, polymer-inorganic, or inorganic-metal hybrid materials have been used in these devices to simultaneously enhance performance and rigidity; yet, understanding which properties, e.g. surface energies or Young's moduli, dictate the mechanical behavior is limited. Numerous experiments using a wide range of techniques have been reported to study the mechanical properties of films nanometers in thickness.[1–36] Most have focused on the variation in glass transition temperature (T_g) or Young's modulus as a function of film thickness.[5,14,17,20,21,28,36–50] Experimental results on T_g are varied, and this is still a topic of debate.[2,4–6,14,17,19,40,45,51,52] Experimental results on the Young's moduli of single layer films have suggested a decrease in the elastic modulus when the thickness of the film was below a critical value, dependent, though, on the experimental technique used.[21,28,48–50,53,54] To remove the residual shear stresses from films on solid substrates, studies have also been performed on liquid surfaces to measure compliance, T_g, elastic modulus, strain, viscosity and dewetting.[2,33,45,55–58] A recent review article discusses many mechanical and rheological methods to determine the material properties of glassy polymers under confinement.[59] Mechanical properties have been determined by the wrinkling of thin films floating on liquid surface, using an out-of-plane deformation. Consequently, tangential shear stresses in the film from the substrate are removed, and the deformation is easily measured by non-contact

probes. The reversibility of the deformation in the linear elasticity regime is simply confirmed by removing the external perturbation.

Here, we investigated the stretching (Y) and bending (B) moduli of unconstrained, stress-relaxed PS/PMMA and PS/Au bilayers using capillary wrinkling. Bilayer films were floated onto water and a drop of water in the center of the film induced a wrinkle pattern. Y and B were determined from the characteristics of the wrinkling pattern using a Far-from-Threshold (FT) analysis of the wrinkling instability.[60] From these two pairs of materials we investigated the influence of surface energies and bulk moduli on the mechanical properties of the bilayer. The total thicknesses of the bilayer films varied from 34 nm to 884 nm for PS/PMMA films, and from 49.6 nm to 495 nm for PS/Au films. The ratio of the thickness of the two layers in the film was also varied over a large range. For both types of films, capillary forces were generated with the PS or PMMA layer, in one case, or the PS or Au layer, in the case, in contact with the underlying liquid. Y and B of the films, determined from the length and number of wrinkles, compare well with those calculated from a weighted average using the bulk Young's moduli of the individual layers. This is meaningful since the results show that the appropriately thickness-weighted averages of Y and B in equation (2) and (4) can estimate the mechanical properties of bilayer thin films. In addition, this also shows that this metrology can be a useful approach to understand the mechanical behaviors of bilayer thin films, broadening scopes of the fin-thin film metrology.

Experimental Methods

PMMA (M_w = 99.6 Kg/mol, with a syndio:hetero:isotactic content of 55:37:8) and poly(acrylic acid) (PAA) solution (Mw ~ 100 Kg/mol, 35 wt% in water) were purchased from

Sigma-Aldrich. PS (M_w = 97 Kg/mol, M_w/M_n = 1.06) was purchased from Polymer Source. Gold pellets (1/4″ Diameter × 1/4″ Length, purity 99.999%) were purchased from Kurt J. Lesker. PS and PMMA were used without further purification. PS was dissolved in either toluene (anhydrous, 99.8%, Sigma-Aldrich) or 1-chloropentane (99%, Sigma-Aldrich) to produce concentrations varying from 0.8 to 7 wt %. PMMA was dissolved in anisole (Anhydrous, 99.8%, Sigma-Aldrich) to produce 0.8 to 6 wt%. solutions of PMMA.[61]

To construct PS(top)/PMMA(bottom) bilayers, a sequential spin-coating onto 3 cm × 3 cm Si substrates with a 250 nm oxide layer was used, since 1-chloropentane is a good solvent for PS and a non-solvent for PMMA. The Si substrates were cleaned using a carbon dioxide snow jet and UV-Ozone (JElight, Model No.342) for 10 minutes before use. Solutions were filtered through 0.45 mm Whatman PTFE filters to remove impurities and then directly applied to the substrate. Different spin-coating speeds (1200 to 4000 rpm) were used to vary the layer thicknesses (47.5 nm to 810.4 nm). The spin-coated films were dried under ambient conditions for 2 days to remove residual solvent and stress. A water-transfer method was also used to produce PMMA/PS bilayer films. PS and PMMA films were spin-coated on separate, pre-cleaned silica wafers. The spin-coated and dried PMMA film were floated onto the surface of water and retrieved on a substrate coated with the dried PS film. The bilayer films were dried under ambient conditions to remove residual water.[62] Various concentrations of solution (0.6 wt% ~ 5.5 wt%) and a wide range of spinning speeds (1200 rpm ~ 4000 rpm) were used to vary the total thicknesses of the PMMA/PS and PS/PMMA (33.6 nm to 884.3 nm) bilayer films.

PS/Au and Au/PS bilayer films were constructed using different methods. The Au (Top)/PS (bottom) bilayer films were obtained by sequentially spin-coating and thermal

evaporation. Solutions with different PS concentrations in toluene (1.8 ~ 5.5 wt%) were filtered and spin-coated onto pre-cleaned substrates at varying spinning speeds (1000 to 6000 RPM) to control the thicknesses of the PS layer. The spin-coated PS films were then dried under ambient conditions for 2 days to remove residual solvent and stress. Au films were thermally evaporated onto spin-coated PS films. Under the evaporation conditions used, the Au at the surface of PS film was consistently measured as 60 °C, avoiding annealing the films above the T_g of PS film. To prepare a bilayer with PS (top)/Au (bottom), a 35 wt% solution of PAA in water was diluted to 5 wt% with deionized water. This was spin coated onto the 3x3 cm^2 substrate to produce a 100 nm thick PAA film, then annealed at 140 °C for 1.5 mins to remove residual water. A 20 nm ± 3.9 nm layer of Au was thermally evaporated onto the PAA film to produce the bilayer. Absent the water-soluble PAA layer, the poor adhesion between the silica substrate and thermally evaporated Au film led to multiple fractures of the Au film when floated onto a water surface. PS solutions with different concentrations (1 ~ 5.5 wt%) were dissolved in toluene. The PS solutions were spin-coated onto the 20 ± 3.9 nm thick Au films to produce PS/Au bilayer films with thicknesses from 49.6 nm to 452.3 nm. The PS/Au bilayer films were dried for 2 days to remove residual stress and solvent.

Bilayer films were cut into 15 mm diameter disks using a tungsten carbide scribe and floated onto the surface of water. A 0.2~ 0.3 µl water droplet was placed at the center of the floating bilayer film with a microsyringe (Hamilton, CAT#80383). The volume of the droplet was then increased in 0.2 µl increments until a maximum volume of ~ 1 µl. Images of the resultant wrinkle pattern at each droplet size were taken with a digital single-lens reflex camera (Nikon D7100) mounted on a stereo microscope (Olympus SZ 40). The images were analyzed using ImageJ and MATLAB to

determine the length and number of wrinkles. After measurement, the bilayer films were retrieved with a silicon substrate using a pre-cleaned 250 nm thick SiO_2 layer and dried for 2 ~ 3 days to remove all the residual water for storage or future use. The film thicknesses of the dried bilayer films were determined using a Filmetrics F20-UV spectral reflectance interferometer.

DATA ANALYSIS

Stretching (Y) and Bending (B) moduli of bilayer films

The mechanical moduli for bilayer films can be determined from those for single layer films. For the stretching modulus, we have the expressions below[62,63]:

$$Y_{Single} = Et \qquad (1)$$

$$Y_{Bi} = E_1 t_1 + E_2 t_2 \qquad (2)$$

where E is the Young's modulus, and t is the film thickness. Subscripts 1 and 2 indicate top and bottom layer s, respectively, of the floating bilayer. The physics behind the expression for the bilayer stretching modulus is relatively transparent, representing the two layers as springs that are in parallel. The in-plane stresses are different in the layers, but the displacement is continuous at the boundary between the layers, if the two layers are in intimate contact. The bending moduli are determined from:

$$B_{Single} = \frac{Et^3}{12(1-\Lambda^2)} \qquad (3)$$

$$B_{Bi} = \frac{E_1 t_1 E_2 t_2 (\frac{t_1+t_2}{2})^2}{(1-{\Lambda_2}^2)E_1 t_1 + (1-{\Lambda_1}^2)E_2 t_2} + \frac{1}{12}\left[\frac{E_1 {t_1}^3}{1-{\Lambda_1}^2} + \frac{E_2 {t_2}^3}{1-{\Lambda_2}^2}\right] \qquad (4)$$

where Λ is the Poisson ratio for the bulk material .[63–65] When a homogeneous film is bent through a radius of curvature, then the outer surface of the film is under tension, while the inner surface is under compression. In the interior of the film, there is an imaginary plane known as the neutral plane, which is unstressed. Integrating through the thickness of the film yields the equation (3) for the bending rigidity of a uniform film. Similar considerations apply to bending a double layer, however, if there is a contrast in the Young's modulus of the two layers, more of the strain resides in the softer material, and the neutral plane is shifted accordingly. This leads to a non-trivial weighting between bending rigidities of 1 and 2 in equation (4) for the bending rigidity of the composite bilayer. Note that bending in either direction carries the same value of B, and this is a considerable simplification as a wrinkle pattern involves alternating the sign of the curvature from peak to valley and back to peak. These formulae assume that (i) there are no finite-thickness effects due to the R_g of the polymer and that the bulk value of Young's modulus can be used for the thin films, (ii) the films are well-bonded to one another, with no relative displacement at the interface between the films, and (iii) the surface on which the capillary force is applied can be accounted for by using the appropriate wetting angles and surface energies. These assumptions will be tested by comparing the predictions with experimentally determined values of Y and B.

The relevant bulk material properties obtained from the literature for our materials are E_{PS} = 3.4 GPa, E_{PMMA} = 3.0 GPa, E_{Au} = 72 GPa, $\Lambda_{PS\ or\ PMMA}$ = 0.34, Λ_{Au}=0.42. The thicknesses of the films were varied over a large range in our experiments.

Extracting bending and stretching modulus from wrinkling patterns

Whenever there is a large enough compressive stress in a thin film, wrinkles form orthogonal to the compression direction. When a film is floating on the surface of water, it

experiences a radial tension at its outer edge equal to the air-water tension (γ), and independent of the solid-liquid surface energy.[66] When a drop of liquid is placed on top of the floating film, there is an out-of-plane capillary force at the contact line, which leads to a boundary condition on the radial stress at the outer edge of the drop. These differential radial tensions on the outside and inside of the film can lead to a compressive tension $\sigma_{\theta\theta}$ in the azimuthal, or hoop, direction.[67] The azimuthal compression leads to the formation of wrinkles along the radial direction. When the scale of the capillary stresses (set by γ) is much larger than the characteristic buckling thresholds for the film, then it is no longer appropriate to use linear stability analysis to infer the size and wave number of the wrinkling patten, but rather, a Far-from-Threshold (FT) analysis must be used. The FT predictions for the wrinkle length shown in equation (5) below are based on the assumption that, to first order, the wrinkles come at no energetic cost (B=0) and relax the compressive stress completely ($\sigma_{\theta\theta=0}$).[60] Thus, the length of the wrinkles depends purely on Y in the limit of very thin films. At the next level of approximation, the finite cost of wrinkling due to a finite B is balanced against the energetic cost of deforming the subphase (gravitational potential energy of the water) and pulling against the radial tension. Thus, the number of wrinkles depends on B, and on the overall radial state of tension.

Within this framework, the length of wrinkles, L, in the Far-from-Threshold (FT) regime was determined as described elsewhere.[60,67,68] The hoop ($\sigma_{\Theta\Theta}$) and radial (σ_{rr}) stresses were calculated from the Lamé solution in a disc geometry under radial stress conditions, and from this, the length L of the wrinkles is predicted as a function of the applied capillary stress

$$L = \frac{\tau a}{2} \qquad (5)$$

where τ is the confinement parameter given in equation (7) below and *a* is the radius of the water droplet on the film.

As previously reported, the number of wrinkles can be approximated using a ″local λ″ law which estimates the wrinkle number as a function of the effective stiffness of the floating film under tension.[68,69] The theory, which incorporates both gravitational potential energy of the water and the radial tension in the film as stiffness terms that oppose the deformation of the film, predicts N(r), the number of wrinkles as a function of radial distance from the contact line as:

$$N(r) \approx r\left[\frac{\rho g+\left(\frac{\tau\gamma_{bath}a}{4r^3}\right)\left(\frac{\log(L/r)-1}{\log(L/r)}\right)^2}{B}\right]^{1/4} \quad (6)$$

$$\tau \approx \frac{\gamma}{\gamma_{bath}}\left(\frac{3}{10}\frac{\sin^2\theta}{x|lnx|}\right)^{\frac{1}{3}} \quad (7)$$

where ρ is the density of water (ρ = 1000 kg/m^3), *g* is gravitational acceleration (g = 9.81 m/s^2), γ_{bath} and γ are both identical in our case, and equal to the surface tension of water since both the bath and the drop contain the same liquid, *a* is the radius of water droplet, θ is the contact angle of the water droplet on the top surface of the film, and $x = (\gamma/Y)$ where Y is the stretching modulus of the bilayer film. Physically, the confinement parameter, τ, is the ratio of the radial stresses at the edge of the drop, and at the outer edge of the film: $\tau \equiv {\sigma_{rr}}^{(a)}/\gamma$.

The theoretical prediction for *N* is a function of the radial distance from the edge of the drop, however, as shown in Fig. 1, the number of wrinkles is uniform in the bulk of the wrinkle pattern. We apply these predictions to the measured wrinkle number at a radial distance halfway through the wrinkle pattern, i.e. at a radial distance given by r=(*a*+*L*)/2. The effective stretching modulus

obtained from the wrinkle length, $Y_{eff,}$, as a function of Y, and the effective bending modulus, B_{eff}, measured from the wrinkle number as a function of B were calculated for PS/PMMA, PMMA/PS, PS/Au, and Au/PS bilayer films using equation (2) for Y, equation (5) and (7) with the Nsolve function in Mathematica for $Y_{eff,}$, equation (4) for B, and equation (6) and (7) for B_{eff}, respectively.

Result and Discussion

Figure 1 (a-d)

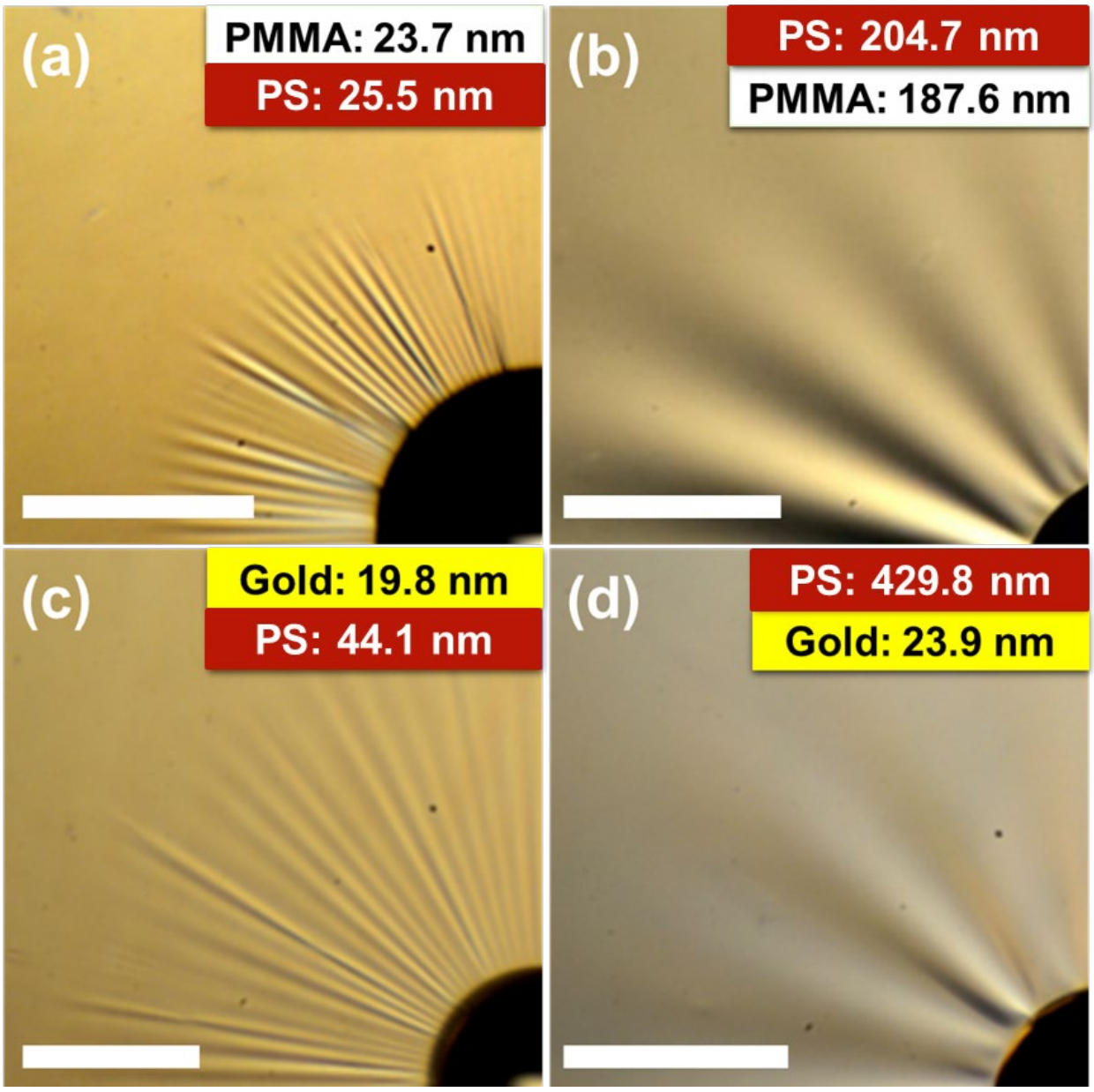

Figure 1. Wrinkle patterns on (a) a PMMA (top)/PS (bottom) thin bilayer film (t_{total}= 49.2 nm), (b) a PS /PMMA bilayer film (t_{total}= 392.3 nm), (c) an Au /PS thin bilayer film (t_{total}= 63.9 nm), (d) a PS/Au (PS/Au) bilayer film (t_{total}= 453.7 nm). Only one quadrant of the film is shown in each case. The drop is seen at the bottom right edge of each image, but the outer edges of the floating film are outside the image. Scale bars are all 1 mm.

Figure 1 shows optical micrographs of the wrinkle patterns of PMMA (Top)/PS (Bottom), PS/PMMA, Au/PS and PS/Au bilayer films where it is seen that the number of wrinkles decreases, and the length of wrinkles increases as the film becomes stiffer. The dominant effect on both bending and in-plane rigidity comes from the thickness of the film. The bulk Young's moduli of the materials are important, and subtler effects appear via the contact angle.

Figure 2 (a-b)

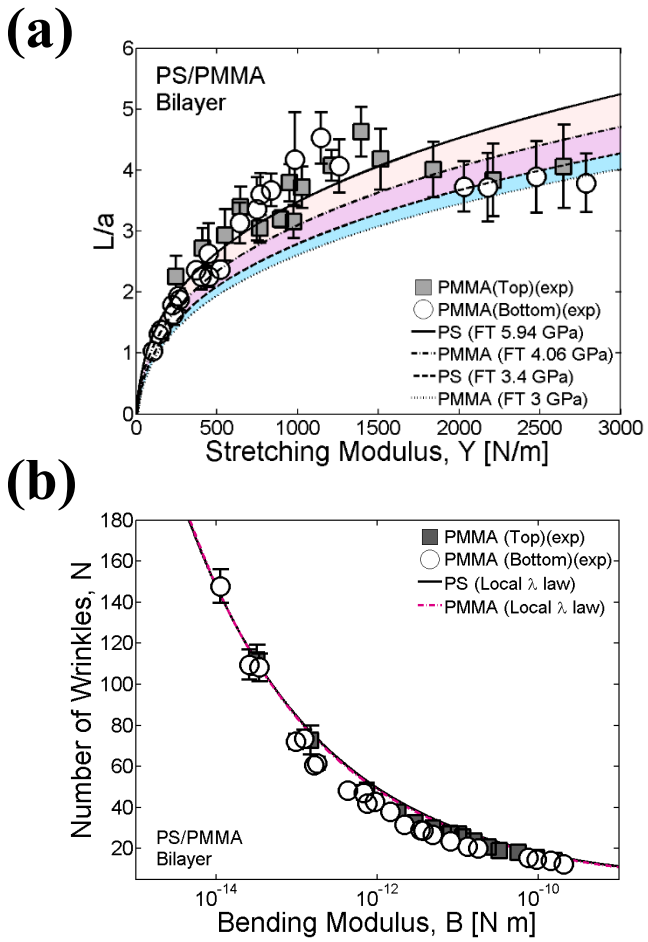

Figure 2. (a) Normalized length of wrinkles (L/*a*) versus stretching modulus (Y) of PS/PMMA and PMMA/PS bilayer films. Lines are calculated from equation (1), (5) and (7) using $E_{PS,exp}$ = 5.9 GPa and $\theta_{PS,}$ = 88° for a solid line, $E_{PMMA,exp}$ = 4.06 GPa and θ_{PMMA} = 68° for a dash-dotted line, $E_{PS,lit}$ = 3.4 GPa and θ_{PS} = 88° for a dashed line, and $E_{PMMA,lit}$ = 3.0 GPa and θ_{PMMA} = 68° for a dotted line, respectively. (b) Number of wrinkles (N) versus bending modulus (B) of PS/PMMA and PMMA/PS bilayer systems. Black solid and red dash-dotted lines are obtained from equation (1), (3), (6) and (7) using $E_{PS,lit}$ = 3.4 GPa, $E_{PMMA,lit}$ = 3.0 GPa, and θ_{PS} = 88° for the black solid line and $E_{PS,lit}$ = 3.4 GPa, $E_{PMMA,lit}$ = 3.0 GPa and θ_{PMMA} = 68° for the red dash-dotted line, respectively.

Figure 3 (a-b)

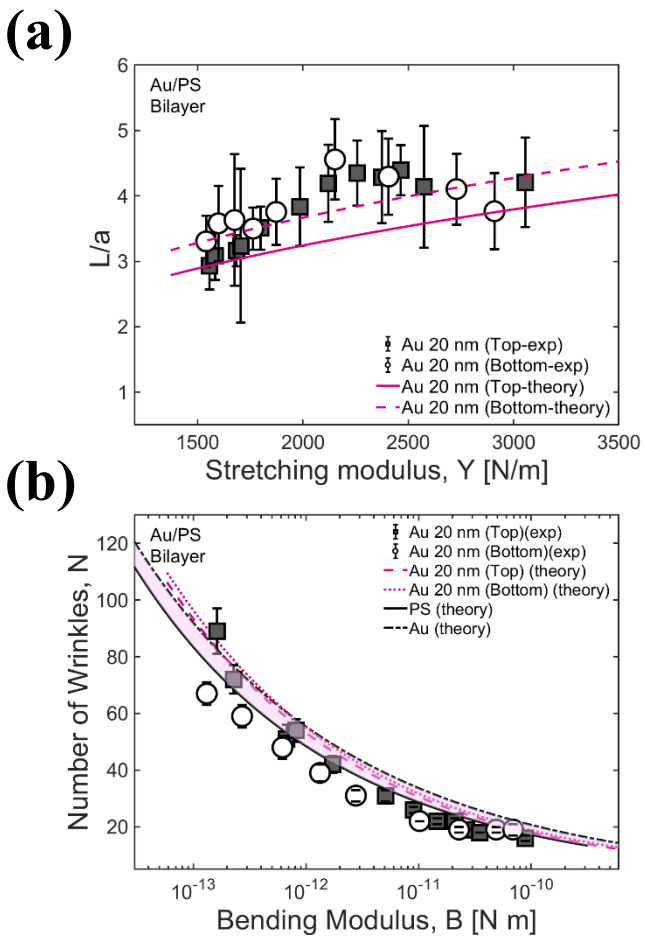

Figure 3. (a) Normalized length of wrinkles (L/*a*) versus stretching modulus (Y) of PS/Au and Au/PS bilayer films. Lines are calculated from equation (2), (5) and (7) using $E_{PS,lit}$ = 3.4 GPa, $E_{Au,lit}$ = 72 GPa, and θ_{Au} = 60° for a red solid line, $E_{PS,lit}$ = 3.4 GPa, $E_{Au,lit}$ = 72 GPa, and θ_{PS} = 88° for a red dash-dotted line, respectively. (b) Number of wrinkles (N) versus bending modulus (B) of PS/Au and Au/PS bilayer systems. Black solid and dash-dotted lines are obtained from equation (1), (3), (6) and (7) using $E_{PS,lit}$ = 3.4 GPa and θ_{PS} = 88°, and $E_{Au,lit}$ = 72 GPa and θ_{Au} = 60°, while red dashed and dotted lines are calculated using equation (2), (4), (6) and (7) with $E_{PS,lit}$ = 3.4 GPa, $E_{Au,lit}$ = 72 GPa, and θ_{PS} = 88°, and $E_{PS,lit}$ = 3.4 GPa, $E_{Au,lit}$ = 72 GPa and θ_{Au} = 60°, respectively.

In Figure 2 (a) and 3 (a) we plot the normalized length (L/a) of the wrinkles in PS/PMMA and PS/Au bilayers, respectively. These are plotted against the expected effective stretching modulus Y, as calculated from the known elastic moduli and the chosen thicknesses of each of the two components in the bilayer, using equation (2). Apart from the thicknesses of the film layers, the other experimental control variable is the drop radius, a. We confirmed that, as in previous work, the length L scales linearly with a, so the normalization in terms of L/a leaves no further dependence on a to account for.[23] Both in Figure 2 (a) and 3 (a), within the error of the measurement, there is no noticeable difference between when one or the other of the two materials is on top. Thus, the dependence that enters through the contact angle does not make a strong difference. The lines in Figures 2 (a) and 3 (a) are theoretical curves from equation (1), (5) and (7) for Figure 2 (a) and equation (2), (5) and (7) for Figure 3 (a), calculated with $E_{PS,experiment\ (exp)}$ = 5.94 GPa, $E_{PS,literature\ (lit)}$ = 3.4 GPa, θ_{PS} = 88°; $E_{PMMA,exp}$ = 4.06 GPa, $E_{PMMA,lit}$ = 3.0 GPa, θ_{PMMA} = 68°, $E_{Au,lit}$ = 72 GPa, and θ_{Au} = 60° [68,70] Note that there are two curves for each bilayer system, corresponding to different experiments with different surfaces of the bilayer facing up, so that different values of the Young-Dupré angle θ need to be inserted in equation (5) and (7). In Figure 2 (a), we show two values of the Young's moduli for both PS and PMMA, one taken from literature on the bulk value, and another determined by us from measurements on single layer films made by the same spin-coating protocols.[68] As can be seen, there is reasonable agreement between the prediction of equation (5) and the observations in Fig 2(a) and 3(a). The largest disagreements are in Figure 2(a) at large values of Y, where the normalized wrinkle length (L/a) increases initially with thickness as expected but saturates for thicker films. We suggest that the saturation arises from a finite size effect, where the length of the wrinkle approaches the size of the bilayer film, whereas our expressions assume a film size much larger than the size of the wrinkle pattern.

In Figure 2 (b) and Figure 3 (b), we plot the measured wrinkled number N(r), evaluated at the middle of the wrinkle pattern, against the expected value of the effective bending modulus B for the bilayer, calculated using equation (4). Once again, the smooth curves in each of the figures correspond to predictions from equation (1), (3), (6) and (7) for Figure 2 (b) and equation (1), (2), (3), (4), (6) and (7) for Figure 3 (b). The predictions for the measured wrinkle number N, match the measurements reasonably well over a very large range of B (4 orders of magnitude for PS/PMMA and PMMA/PS bilayer films and 3 orders of magnitude for the PS/Au and Au/PS films). There are small, but systematic differences between the PS/Au and Au/PS bilayers, which we note were made by entirely different protocols.

Figure 4 (a-b)

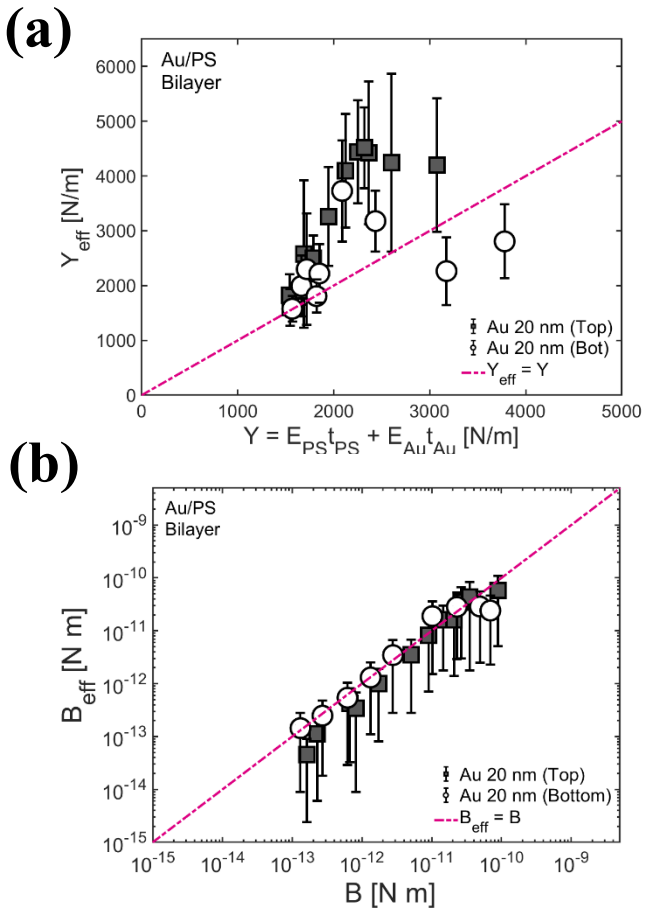

Figure 4. (a) Theoretical stretching modulus, Y, dependence of the effective stretching modulus, Y_{eff}, obtained from Au/PS and PS/Au bilayer films. Y was determined with equation (2) and Y_{eff} was quantified utilizing the experimental wrinkle lengths with equation (5) and (7). (b) Theoretical bending modulus, B, dependence of the effective bending modulus, B_{eff}, measured with Au/PS and PS/Au bilayer films. The B and B_{eff} values were computed using equation (4) for B and equation (6) and (7) for B_{eff}, respectively. $E_{PS,lit}$ = 3.4 GPa, $E_{Au,lit}$ = 72 GPa, t_{Au} = 20 nm and a t_{PS}, 29.6 nm $\leq t_{PS} \leq$ 475.2 nm, were used to calculate Y, Y_{eff}, B, and B_{eff}.

As an example, Figure 4 (a) and (b) we show the comparison in a different way for the polymer-gold system. Here we compare the experimentally measured values of the effective stretching moduli (Y_{eff}) and bending moduli (B_{eff}) (i.e. by using experimentally measured L and N, and numerically inverting equation (5) and (7) for Y_{eff} and equation (6) and (7) for B_{eff}) to the ones calculated from equation (2) and (4) based on the known Young's moduli of PS and Au and film thicknesses. The experimental Y_{eff} and B_{eff} are comparable to the calculated values, Y_{eff} is higher than Y, yet, B_{eff} is systematically lower for Au/PS bilayer films where $B \leq \sim 10^{-11}$ N·m.[71,72] The calculation that results in equation (5), (6) and (7) which enable our ability to determine Y and B from L and N(r), ignores some details that can have quantitative effects: first, the displacement boundary conditions at r=a are quite complex in the experiment. Second, there is a boundary layer at the tip of the wrinkle where the curved portion meets the planar part of the film; this can contribute to the observed length of the wrinkle but is not included in equation (5), (6) and (7).[68]

Conclusion

Our results show that the bending and stretching moduli of bilayer films, both polymer/polymer and polymer/Au, can be correctly determined knowing the individual thicknesses and Young's moduli of the two layers. The moduli estimated from equations 1 and 2 agree well with the moduli determined in our experimental data for the size and wave number of wrinkle patterns generated by capillary stresses. We have explicitly tested this agreement over a broad range of total film thickness for PMMA/PS and PS/PMMA (33.6 nm to 884.3 nm), and for PS/Au and Au/PS (49.6 nm to 495.2 nm) and ratios of the individual layer thicknesses. We account for the contrasts in wetting properties with different contact angles of θ_{PMMA} = 68 º, θ_{PS} = 88 º and θ_{Au} = 60 º mechanical properties accompanied by different Young's moduli of E_{PS} = 3.4 GPa and E_{Au} = 72 GPa. Stretching and bending moduli for the PMMA/PS and PS/PMMA bilayer films responded like a single elastic object, with no slippage at the interface between the two layers. This was also found to be true for PS/Au and Au/PS bilayer films, we do however, see a small but systematic difference between these two types of film possibly because they were synthesized by entirely different protocols. From these results, we show that the combination of a classic bilayer model with classic formulae (Y and B) can be used to determine the mechanical properties of the bilayer films. In addition, these findings can be useful in cases where non-bulk effects are anticipated, widening perspectives beyond thin-film metrology.

Acknowledgement

This work was supported by the by the US Army Research Office under contract W911NF-24-2-0041, the W.M. Keck Foundation, and NSF grants 2226310 and 1905698. We thank Y. Kim,

B. Davidovitch, D. Vella, D. Kumar, Y. Liu, H. Lee, D. Waldman, S. Chantarak, J. Choi, J. Patel, D.M. Yu, H. Kim, S. Srivastava, Z. Fink, S. Lee, I. Chang and E. Chang for fruitful discussions.

References

(1) Brown, H. R.; Russell, T. P. Entanglements at Polymer Surfaces and Interfaces. *Macromoelcules* **1996**, *29*, 798–800. https://doi.org/10.1021/ma951123k.

(2) Lu, H.; Chen, W.; Russell, T. P. Relaxation of Thin Films of Polystyrene Floating on Ionic Liquid Surface. *Macromolecules* **2009**, *42*, 9111–9117. https://doi.org/10.1021/ma901789k.

(3) Plazek, D. J. Temperature Dependence of the Viscoelastic Behavior of Polystyrene. *Journal of Physical Chemistry* **1965**, *69*, 3480–3487. https://doi.org/10.1021/j100894a039.

(4) Alcoutlabi, M.; McKenna, G. B. Effects of Confinement on Material Behaviour at the Nanometre Size Scale. *Journal of Physics: Condensed Matter* **2005**, *17*, R461–R524. https://doi.org/10.1088/0953-8984/17/15/R01.

(5) Yoon, H.; Mckenna, G. B. Substrate Effects on Glass Transition and Free Surface Viscoelasticity of Ultrathin Polystyrene Films. *Macromolecules* **2014**, *47*, 8808–8818. https://doi.org/10.1021/ma501630g.

(6) Li, X.; McKenna, G. B. Ultrathin Polymer Films: Rubbery Stiffening, Fragility, and T g Reduction. *Macromolecules* **2015**, *48*, 6329–6336. https://doi.org/10.1021/acs.macromol.5b01263.

(7) Majeste, J. C.; Montfort, J. P.; Allal, A.; Marin, G. Viscoelasticity of Low Molecular Weight Polymers and the Transition to the Entangled Regime. *Rheol Acta* **1998**, *37*, 486–499. https://doi.org/10.1007/s003970050135.

(8) King, H.; Schroll, R. D.; Davidovitch, B.; Menon, N. Elastic Sheet on a Liquid Drop Reveals Wrinkling and Crumpling as Distinct Symmetry-Breaking Instabilities. *Proceedings of the National Academy of Sciences* **2012**, *109*, 9716–9720. https://doi.org/10.1073/pnas.1201201109.

(9) King, J. S.; Boyer, W.; Wignall, G. D.; Ullman, R. Radii of Gyration and Screening Lengths of Polystyrene in Toluene as a Function of Concentration. *Macromolecules* **1985**, *18*, 709–718. https://doi.org/10.1021/ma00146a023.

(10) Cerda, E.; Mahadevan, L. Geometry and Physics of Wrinkling. *Phys Rev Lett* **2003**, *90* (7), 074302. https://doi.org/10.1103/PhysRevLett.90.074302.

(11) Xia, W.; Keten, S. Interfacial Stiffening of Polymer Thin Films under Nanoconfinement. *Extreme Mech Lett* **2015**, *4*, 89–95. https://doi.org/10.1016/j.eml.2015.05.001.

(12) Vella, D.; Adda-Bedia, M.; Cerda, E. Capillary Wrinkling of Elastic Membranes. *Soft Matter* **2010**, *6*, 5778. https://doi.org/10.1039/c0sm00432d.

(13) Paeng, K.; Ediger, M. D. Molecular Motion in Free-Standing Thin Films of Poly(Methyl Methacrylate), Poly(4-Tert-Butylstyrene), Poly(α-Methylstyrene), and Poly(2- Vinylpyridine). *Macromolecules* **2011**, *44*, 7034–7042. https://doi.org/10.1021/ma201266r.

(14) Lee, H.; Paeng, K.; Stephen F. Swallen, M. D. E. Direct Measurement of Molecular Mobility in Actively Deformed Polymer Glasses. *Science (1979)* **2009**, *323*, 231–234. https://doi.org/10.1126/science.1165995.

(15) Paeng, K.; Swallen, S. F.; Ediger, M. D. Direct Measurement of Molecular Motion in Freestanding Polystyrene Thin Films. *J Am Chem Soc* **2011**, *133*, 8444–8447. https://doi.org/10.1021/ja2022834.

(16) Rittigstein, P.; Priestley, R. D.; Broadbelt, L. J.; Torkelson, J. M. Model Polymer Nanocomposites Provide an Understanding of Confinement Effects in Real Nanocomposites. *Nat Mater* **2007**, *6*, 278–282. https://doi.org/10.1038/nmat1870.

(17) Priestley, R. D.; Ellison, C. J.; Broadbelt, L. J.; Torkelson, J. M. Structural Relaxation of Polymer Glasses at Surfaces, Interfaces, and in Between. *Science (1979)* **2005**, *309*, 456–459. https://doi.org/10.1126/science.1112217.

(18) Roth, C. B.; McNerny, K. L.; Jager, W. F.; Torkelson, J. M. Eliminating the Enhanced Mobility at the Free Surface of Polystyrene: Fluorescence Studies of the Glass Transition Temperature in Thin Bilayer Films of Immiscible Polymers. *Macromolecules* **2007**, *40*, 2568–2574. https://doi.org/10.1021/ma062864w.

(19) Ellison, C. J.; Torkelson, J. M. The Distribution of Glass-Transition Temperatures in Nanoscopically Confined Glass Formers. *Nat Mater* **2003**, *2*, 695–700. https://doi.org/10.1038/nmat980.

(20) Torres, J. M.; Stafford, C. M.; Vogt, B. D. Elastic Modulus of Amorphous Polymer Thin Films: Relationship to the Glass Transition Temperature. *ACS Nano* **2009**, *3*, 2677–2685. https://doi.org/10.1021/nn9006847.

(21) Torres, J. M.; Stafford, C. M.; Vogt, B. D. Impact of Molecular Mass on the Elastic Modulus of Thin Polystyrene Films. *Polymer (Guildf)* **2010**, *51*, 4211–4217. https://doi.org/10.1016/j.polymer.2010.07.003.

(22) Bowden, N.; Brittain, S.; Evans, A. G.; Hutchinson, J. W.; Whitesides, G. M. Spontaneous Formation of Ordered Structures in Thin Films of Metals Supported on an Elastomeric Polymer. *Nature* **1998**, *393*, 146–149. https://doi.org/10.1038/30193.

(23) Huang, J.; Juszkiewicz, M.; De Jeu, W. H.; Cerda, E.; Emrick, T.; Menon, N.; Russell, T. P. Capillary Wrinkling of Floating Thin Polymer Films. *Science (1979)* **2007**, *317*, 650–653. https://doi.org/10.1126/science.1144616.

(24) Toga, K. B.; Huang, J.; Cunningham, K.; Russell, T. P.; Menon, N. A Drop on a Floating Sheet: Boundary Conditions, Topography and Formation of Wrinkles. *Soft Matter* **2013**, *9*, 8289–8296. https://doi.org/10.1039/C3SM50736J.

(25) Kerle, T.; Lin, Z.; Kim, H.; Russell, T. P. Mobility of Polymers at the Air / Polymer Interface. *Macromolecules* **2001**, *34*, 3484–3492. https://doi.org/10.1021/ma0020335.

(26) Jones, R.; Kumar, S.; Ho, D.; Briber, R.; Russell, T. Chain Conformation in Ultrathin Polymer Films. *Nature* **1999**, *400*, 146–149. https://doi.org/10.1038/22080.

(27) Stafford, C. M.; Harrison, C.; Beers, K. L.; Karim, A.; Amis, E. J.; VanLandingham, M. R.; Kim, H.-C.; Volksen, W.; Miller, R. D.; Simonyi, E. E. A Buckling-Based Metrology for Measuring the Elastic Moduli of Polymeric Thin Films. *Nat Mater* **2004**, *3*, 545–550. https://doi.org/10.1038/nmat1175.

(28) Stafford, C. M.; Vogt, B. D.; Harrison, C.; Julthongpiput, D.; Huang, R. Elastic Moduli of Ultrathin Amorphous Polymer Films. *Macromolecules* **2006**, *39*, 5095–5099. https://doi.org/10.1021/ma060790i.

(29) O'Connell, P. A.; McKenna, G. B. Rheological Measurements of the Thermoviscoelastic Response of Ultrathin Polymer Films. *Science (1979)* **2005**, *307*, 1760–1763. https://doi.org/10.1126/science.1105658.

(30) O'Connell, P. A.; Mckenna, G. B. A Novel Nano-Bubble Inflation Method for Determining the Viscoelastic Properties of Ultrathin Polymer Films. *Scanning* **2008**, *30*, 184–196. https://doi.org/10.1002/sca.20088.

(31) O'Connell, P. A.; McKenna, G. B. Dramatic Stiffening of Ultrathin Polymer Films in the Rubbery Regime. *European Physical Journal E* **2006**, *20*, 143–150. https://doi.org/10.1140/epje/i2005-10125-4.

(32) Zhao, J. H.; Kiene, M.; Hu, C.; Ho, P. S. Thermal Stress and Glass Transition of Ultrathin Polystyrene Films. *Appl Phys Lett* **2000**, *77*, 2843–2845. https://doi.org/10.1063/1.1322049.

(33) Liu, Y.; Chen, Y. C.; Hutchens, S.; Lawrence, J.; Emrick, T.; Crosby, A. J. Directly Measuring the Complete Stress-Strain Response of Ultrathin Polymer Films. *Macromolecules* **2015**, *48*, 6534–6540. https://doi.org/10.1021/acs.macromol.5b01473.

(34) Kim, J.-H.; Nizami, A.; Hwangbo, Y.; Jang, B.; Lee, H.-J.; Woo, C.-S.; Hyun, S.; Kim, T.-S. Tensile Testing of Ultra-Thin Films on Water Surface. *Nat Commun* **2013**, *4*, 1–6. https://doi.org/10.1038/ncomms3520.

(35) Forrest, J. A.; Veress, K. D.; Dutcher, J. R. Brillouin Light Scattering Studies of the Mechanical Properties of Thin Freely Standing Polystyrene Films. *Phys Rev E* **1998**, *58*, 6109–6114. https://doi.org/10.1103/PhysRevE.58.6109.

(36) DeMaggio, G.; Frieze, W.; Gidley, D.; Zhu, M.; Hristov, H.; Yee, A. F. Interface and Surface Effects on the Glass Transition in Thin Polystyrene Films. *Phys Rev Lett* **1997**, *78*, 1524–1527. https://doi.org/10.1103/PhysRevLett.78.1524.

(37) Mansfield, K. F.; Theodorou, D. N. Atomistic Simulation of a Glassy Polymer Surface. *Macromolecules* **1990**, *23*, 4430–4445. https://doi.org/10.1021/ma00222a016.

(38) Maillard, D.; Kumar, S. K.; Fragneaud, B.; Kysar, J. W.; Rungta, A.; Benicewicz, B. C.; Deng, H.; Brinson, L. C.; Douglas, J. F. Mechanical Properties of Thin Glassy Polymer Films Filled with Spherical Polymer-Grafted Nanoparticles. *Nano Lett* **2012**, *12*, 3909–3914. https://doi.org/10.1021/nl301792g.

(39) Wallace, W. E.; Van Zanten, J. H.; Wu, W. L. Influence of an Impenetrable Interface on a Polymer Glass-Transition Temperature. *Phys Rev E* **1995**, *52*, R3329–R3332. https://doi.org/10.1103/PhysRevE.52.R3329.

(40) Tsui, O. K. C.; Wang, X. P.; Ho, J. Y. L.; Ng, T. K.; Xiao, X. Studying Surface Glass-to-Rubber Transition Using Atomic Force Microscopic Adhesion Measurements. *Macromolecules* **2000**, *33*, 4198–4204. https://doi.org/10.1021/ma991473x.

(41) Kawana, S.; Jones, R. A. L. Character of the Glass Transition in Thin Supported Polymer Films. *Phys Rev E* **2001**, *63*, 021501. https://doi.org/10.1103/PhysRevE.63.021501.

(42) Tran, T. A.; Saïd, S.; Grohens, Y. Nanoscale Characteristic Length at the Glass Transition in Confined Syndiotactic Poly(Methyl Methacrylate). *Macromolecules* **2005**, *38*, 3867–3871. https://doi.org/10.1021/ma0487296.

(43) Kremer, F.; Tress, M.; Mapesa, E. U. Glassy Dynamics and Glass Transition in Nanometric Layers and Films: A Silver Lining on the Horizon. *J Non Cryst Solids* **2015**, *407*, 277–283. https://doi.org/10.1016/j.jnoncrysol.2014.08.016.

(44) Forrest, J. A.; Dalnoki-Veress, K. The Glass Transition in Thin Polymer Films. *Adv Colloid Interface Sci* **2001**, *94*, 167–196. https://doi.org/10.1016/S0001-8686(01)00060-4.

(45) Wang, J.; McKenna, G. B. Viscoelastic Properties of Ultrathin Polycarbonate Films by Liquid Dewetting. *J Polym Sci B Polym Phys* **2015**, *53*, 1559–1566. https://doi.org/10.1002/polb.23807.

(46) Jones, R. L.; Kumar, S. K.; Ho, D. L.; Briber, R. M.; Russell, T. P. Chain Conformation in Ultrathin Polymer Films Using Small-Angle Neutron Scattering. *Macromolecules* **2001**, *34*, 559–567. https://doi.org/10.1021/ma001141o.

(47) Tweedie, C. A.; Constantinides, G.; Lehman, K. E.; Brill, D. J.; Blackman, G. S.; Van Vliet, K. J. Enhanced Stiffness of Amorphous Polymer Surfaces under Confinement of Localized Contact Loads. *Advanced Materials* **2007**, *19*, 2540–2546. https://doi.org/10.1002/adma.200602846.

(48) Lee, J. H.; Chung, J. Y.; Stafford, C. M. Effect of Confinement on Stiffness and Fracture of Thin Amorphous Polymer Films. *ACS Macro Lett* **2012**, *1*, 122–126. https://doi.org/10.1021/mz200090a.

(49) Stafford, C. M.; Harrison, C.; Beers, K. L.; Karim, A.; Amis, E. J.; Vanlandingham, M. R.; Kim, H. C.; Volksen, W.; Miller, R. D.; Simonyi, E. E. A Buckling-Based Metrology for Measuring the Elastic Moduli of Polymeric Thin Films. *Nat Mater* **2004**, *3*, 545–550. https://doi.org/10.1038/nmat1175.

(50) Page, K. A.; Kusoglu, A.; Stafford, C. M.; Kim, S.; Kline, R. J.; Weber, A. Z. Confinement-Driven Increase in Ionomer Thin-Film Modulus. *Nano Lett* **2014**, *14*, 2299–2304. https://doi.org/10.1021/nl501233g.

(51) Roth, C. B.; McNerny, K. L.; Jager, W. F.; Torkelson, J. M. Eliminating the Enhanced Mobility at the Free Surface of Polystyrene: Fluorescence Studies of the Glass Transition Temperature in Thin Bilayer Films of Immiscible Polymers. *Macromolecules* **2007**, *40*, 2568–2574. https://doi.org/10.1021/ma062864w.

(52) Torkelson, J. M.; Lipsky, S.; Tirrell, M. Polystyrene Fluorescence: Effects of Molecular Weight in Various Solvents. *Macromolecules* **1981**, *14*, 1601–1603. https://doi.org/10.1021/ma50006a094.

(53) Du, B.; Tsui, O. K. C.; Zhang, Q.; He, T. Study of Elastic Modulus and Yield Strength of Polymer Thin Films Using Atomic Force Microscopy. *Langmuir* **2001**, *17*, 3286–3291. https://doi.org/10.1021/la001434a.

(54) Maillard, D.; Kumar, S. K.; Rungta, A.; Benicewicz, B. C.; Prud'Homme, R. E. Polymer-Grafted-Nanoparticle Surfactants. *Nano Lett* **2011**, *11*, 4569–4573. https://doi.org/10.1021/nl202651u.

(55) Bodiguel, H.; Fretigny, C. Reduced Viscosity in Thin Polymer Films. *Phys Rev Lett* **2006**, *97*, 1–4. https://doi.org/10.1103/PhysRevLett.97.266105.

(56) Bodiguel, H.; Fretigny, C. Viscoelastic Dewetting of a Polymer Film on a Liquid Substrate. *European Physical Journal E* **2006**, *19*, 185–193. https://doi.org/10.1140/epje/e2006-00021-8.

(57) Bodiguel, H.; Fretigny, C. Viscoelastic Properties of Ultrathin Polystyrene Films. *Macromolecules* **2007**, *40*, 7291–7298. https://doi.org/10.1021/ma070460d.

(58) Wang, J.; McKenna, G. B. Viscoelastic and Glass Transition Properties of Ultrathin Polystyrene Films by Dewetting from Liquid Glycerol. *Macromolecules* **2013**, *46*, 2485–2495. https://doi.org/10.1021/ma400040j.

(59) Madhusudanan, M.; Chowdhury, M. Advancements in Novel Mechano-Rheological Probes for Studying Glassy Dynamics in Nanoconfined Thin Polymer Films. *ACS Polymers Au* **2024**. https://doi.org/10.1021/acspolymersau.4c00022.

(60) Schroll, R. D.; Adda-Bedia, M.; Cerda, E.; Huang, J.; Menon, N.; Russell, T. P.; Toga, K. B.; Vella, D.; Davidovitch, B. Capillary Deformations of Bendable Films. *Phys Rev Lett* **2013**, *111*, 014301. https://doi.org/10.1103/PhysRevLett.111.014301.

(61) Ennis, D.; Heike, B.; Ade, H. Direct Spincasting of Polystyrene Thin Films onto Poly(Methyl Methacrylate). *J Polym Sci B Polym Phys* **2006**, *44* (22), 3234–3244. https://doi.org/10.1002/polb.

(62) Yoon, H.; McKenna, G. B. Substrate Effects on Glass Transition and Free Surface Viscoelasticity of Ultrathin Polystyrene Films. *Macromolecules* **2014**, *47*, 8808–8818. https://doi.org/10.1021/ma501630g.

(63) Whitney, J. M. *Structural Analysis of Laminated Anisotropic Plates*; Technomic: Lancaster, 1987.

(64) Avilés, F.; Oliva, A. I.; May-Pat, A. Determination of Elastic Modulus in a Bimaterial through a One-Dimensional Laminated Model. *J Mater Eng Perform* **2008**, *17* (4), 482–488. https://doi.org/10.1007/s11665-007-9185-1.

(65) Allen, H. *Analysis and Design of Structural Sandwich Panels.*; Pergamon Press.: New York, 1969.

(66) Kumar, D.; Russell, T. P.; Davidovitch, B.; Menon, N. Stresses in Thin Sheets at Fluid Interfaces. *Nat Mater* **2020**, *19* (7), 690–693. https://doi.org/10.1038/s41563-020-0640-9.

(67) Davidovitch, B.; Schroll, R. D.; Vella, D.; Adda-Bedia, M.; Cerda, E. a. Prototypical Model for Tensional Wrinkling in Thin Sheets. *Proceedings of the National Academy of Sciences* **2011**, *108*, 18227–18232. https://doi.org/10.1073/pnas.1108553108.

(68) Chang, J.; Toga, K. B.; Paulsen, J. D.; Menon, N.; Russell, T. P. Thickness Dependence of the Young's Modulus of Polymer Thin Films Macromolecules. *Macromolecules* **2018**, *51*, 6764–6770. https://doi.org/10.1021/acs.macromol.8b00602.

(69) Paulsen, J. D.; Hohlfeld, E.; King, H.; Huang, J.; Qiu, Z.; Russell, T. P.; Menon, N.; Vella, D.; Davidovitch, B. Curvature-Induced Stiffness and the Spatial Variation of Wavelength in Wrinkled Sheets. *Proceedings of the National Academy of Sciences* **2016**, *113*, 1144–1149. https://doi.org/10.1073/pnas.1521520113.

(70) Wang, L.; Liang, C.; Prorok, B. C. A Comparison of Testing Methods in Assessing the Elastic Properties of Sputter-Deposited Gold Films. *Thin Solid Films* **2007**, *515*, 7911–7918. https://doi.org/10.1016/j.tsf.2007.04.022.

(71) Landau, L.; Lifshitz, E. *Theory of Elasticity*; 1986.

(72) Timoshenko, S.; Goodier, J. N. *Theory of Elasticity*, 3rd ed.; McGraw-Hil: New York, 1969. https://doi.org/10.1007/BF00046464.